Mathematical Sciences and Informatics Journal
Vol. 5, No. 2, Nov. 2024, pp. 57-69
http://www.mijuitm.com.my
DOI : 10.24191/mij.v5i2.926

Total Variation Selective Segmentation-based Active Contour Model with Distance Function and Local Image Fitting Energy for Medical Images

Nadiah Mohamed
School of Mathematical Sciences, College of Computing, Informatics and Mathematics, Universiti Teknologi MARA, Negeri Sembilan Campus, Malaysia
nadiah@uitm.edu.my

Abdul Kadir Jumaat
School of Mathematical Sciences, College of Computing, Informatics and Mathematics, Universiti Teknologi MARA, Shah Alam, Malaysia
Institute for Big Data Analytics and Artificial Intelligence (IBDAAI), Universiti Teknologi MARA, Shah Alam, Selangor, Malaysia
abdulkadir@tmsk.uitm.edu.my

Rozi Mahmud
Radiology Department, Faculty of Medicine and Health Sciences, Universiti Putra Malaysia, Serdang, Selangor, Malaysia
rozi@upm.edu.my

Article Info

Article history:

Received Apr 20, 2024
Revised Aug 18, 2024
Accepted Sept 17, 2024

Keywords:

Active Contour
Total Variation
Image Processing
Image Segmentation
Mathematical Model
Medical Image
Selective Segmentation
Variational Model

ABSTRACT

The Active Contour Model (ACM) is a mathematical model in image processing that is commonly utilized to partition or segment an image into specific objects. The segmentation method in region-based ACM can be categorized into two classes: global ACM and selective ACM Selective ACM isolates a specific target item from an input image, which is more advantageous than the global ACM due to its proven use, particularly in medical image analysis. However, the selective ACM appears to produce poor outcomes when segmenting an image with uneven (inhomogeneous) intensity. Additionally, the current selective ACM that uses the Gaussian function as a regularizer generates a non-smooth segmentation curve, especially for images containing noise. This study introduces a new selective ACM that is designed to segment medical images with inhomogeneous intensity levels. The model incorporates a Total Variation term as a regularizer, distance function, and local image fitting concepts. The Euler-Lagrange (EL) equation was given to solve the suggested model, which is approximately 5% more accurate with a processing time that is around three times faster than the existing model, as shown by numerical testing. The suggested mathematical model can be advantageous for the image analysis community, particularly in the medical industry, to automatically segment a specific object in a medical image.

Corresponding Author:
Abdul Kadir Jumaat
School of Mathematical Sciences, College of Computing, Informatics and Mathematics, Universiti Teknologi MARA, Shah Alam, Malaysia
Institute for Big Data Analytics and Artificial Intelligence (IBDAAI), Universiti Teknologi MARA, 40450, Shah Alam, Selangor, Malaysia
Email: abdulkadir@tmsk.uitm.edu.my

1. Introduction

In image processing field, the image segmentation approach either variational or non-variational approaches is an essential step involves in separating a digital picture into different portions for further investigations in many application such as recognition of object, medical image analysis and computer vision [1-5]. Non-variational approaches such as thresholding and region

PENERBIT PRESS
UNIVERSITI TEKNOLOGI MARA

growth are good for basic images but struggle with topological changes. Another well-known non-variational method namely the learning methods (machine or deep learning) demand a significant quantity of labelled data, which is often not accessible. In contrast, variational methods are less reliant on the quantity of data and additionally they are demonstrated efficacy in picture segmentation.

In variational approaches, the Active contour model (ACM) is a popular method that utilize the calculus of variations to apply optimization strategies to minimize the energy cost function. There are two forms of variational ACM: edge-based and region-based methods. A prominent edge-based variational ACM namely Snake model [6] was formulated in explicit parametric contour. The drawback of this technique is susceptible to picture noise. In contrast, the region-based variational ACM is less affected by image noise and capable to manage topological changing as the method considers statistical features of an input images in the formulation [7-9]. This region-based variational ACM may be categorized into two classes: global ACM and selective ACM.

The most recognized variational global active contour model was the Mumford-Shah model developed in [10]. Being a global type of model, its objective is to segment all items or objects included in the input picture. A simplified version [11] of the Mumford-Shah model into a precise numerical representation known as the Chan-Vese (CV) model. However, the CV model may yield unsatisfactory outcomes as this model's reliance on global image intensity information in its mathematical formulation hinders its ability to effectively segment images that have intensity inhomogeneity.

Intensity inhomogeneity is a significant limitation in image segmentation, especially in medical imaging due to presence of noise or problem with the imaging modalities. This pertains to fluctuations in picture intensity levels within a single image, causing challenges, for instance, in distinguishing between healthy and abnormal tissue that results in erroneous judgements among medical professionals. This may be detrimental, as for disorders like cancer, precise diagnosis is crucial for planning efficient therapy.

2. Literature Review

The Local Binary Fitting (LBF) model [12] was presented to address the issue of segmenting an image with intensity inhomogeneity by including local image intensity. However, the accurate segmentation result achieved by using the LBF model led to longer processing time due to its high computational complexity. Therefore, another ACM model namely Local Image Fitting (LIF) model was proposed [13] to address the shortcomings of the LBF approach. Subsequently, several studies have applied similar concept of LIF model as demonstrated by [14-16]. However, the LIF model cannot be used to segment a particular item in an input picture.

To address the issue of segmenting a particular item in an input picture, the selective segmentation model (selective ACM), which is the second type of variational region-based ACM, is recommended. Selective segmentation is the process of partitioning a particular item in an image into multiple segments based on markers specified by the user. This technique shows promise for integration with medical imaging [17-[8], biometric identification [19], and text analysis [20]. A selective ACM algorithm called Primal Dual Selective Segmentation (PDSS) was introduced in [21]. This approach has been demonstrated to be effective at isolating a particular item within an input image. However, the PDSS model encounters a significant challenge in segmenting pictures with low contrast. Hence, a modified PDSS model called PDSS2 [22], which replaces the fitting term with information obtained from the image enhancement approach to address the issue. Unfortunately, the precise information obtained by the PDSS2 appears inadequate for identifying the near-optimal segmented border of an object with intensity inhomogeneity issues.

Recently, a novel variational selective region-based ACM was introduced in 2023 called the Gaussian regularization selective segmentation (GRSS) model [23] for pictures with intensity inhomogeneity. However, the curve created using a Gaussian kernel regularizer in the formulation was not smooth because the regularizer is sensitive to image noise. Additionally, it is difficult to tune the parameter that control the regularizer. Besides Gaussian kernal function, another more powerful regularizer is to utilize the Total variation (TV) functional. The CV model [11] was an early mathematical model that incorporated TV in its formulation, leading to a smooth segmentation curve. However, as the model was formed inside a variational global region-based segmentation framework, it was not able to effectively segment a specific item in an image.

This study introduces a novel variational selective region-based ACM called the Total Variation based Selective Segmentation (TVSS) model for pictures with intensity inhomogeneity that incorporates the concept of employing TV as a regularizer. In addition, the local attribute of an input picture was included using the concept from the LIF model [13]. A distance function from the GRSS model [23] was used to capture a specific target.

This article is divided into three portions. Section 3 outlines the methodology of the study and introduces the suggested energy function of the proposed model. Section 4 includes a comparison and explanation of the experimental results. Section 5 discusses the findings and recommendations for further research.

3. Methodology

This section outlines the methodology of the study, as depicted in the flow chart shown in Figure 1.

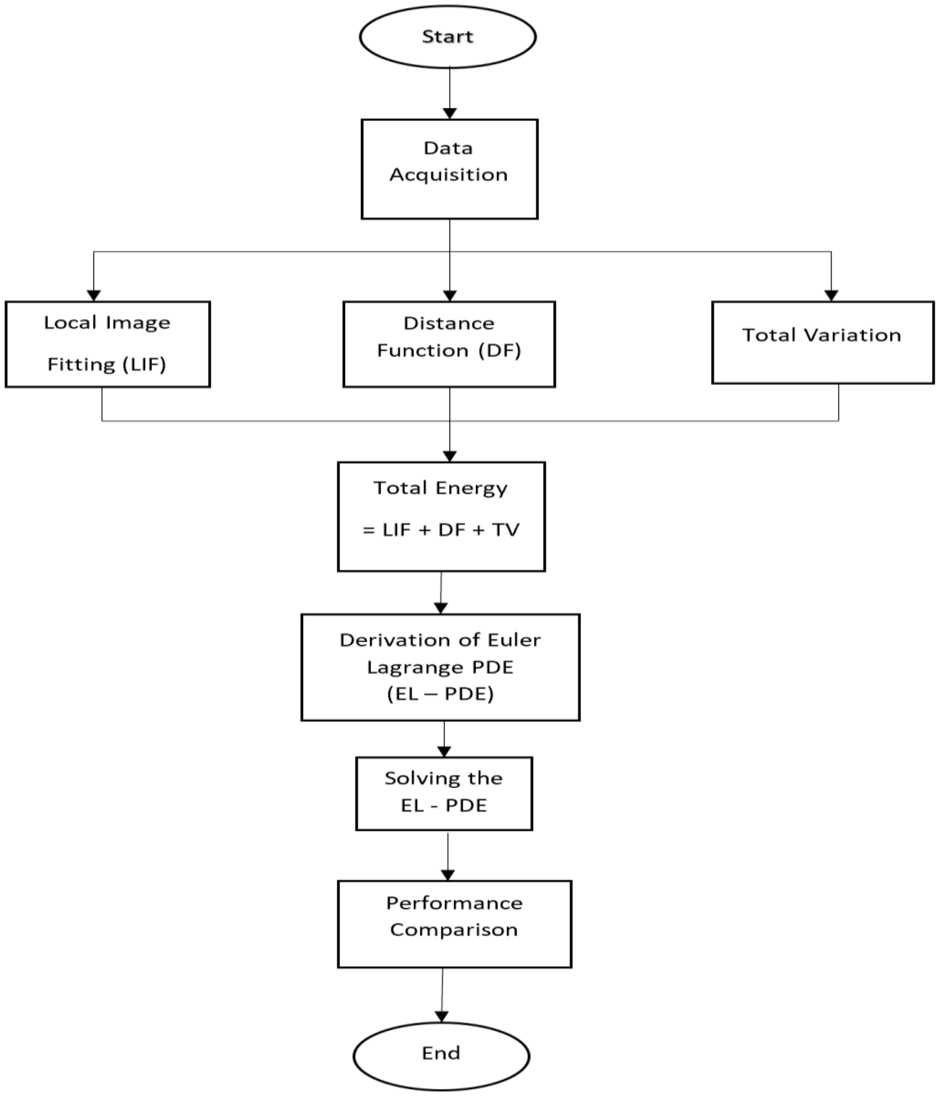

Figure 1. Flowchart of the research methodology

Figure 1 depicts the flowchart outlining the research methodology used in this study. The Local Image Fitting (LIF) energy, Distance Function (DF), and TV of an input picture were calculated at the beginning. A total energy minimization function was created to reflect the suggested TVSS model to segment the input picture. This function integrates the LIF energies, DF, and TV term. The Euler-Lagrange Partial Differential Equation (EL-PDE) of the TVSS model was generated and solved. The performance of the proposed TVSS model was then compared with the GRSS model. In the following section, each stage is described in detail.

3.1 Data Acquisition

In this study, six (6) sets of mammography test images and six (6) sets of chest X-ray test images with their ground truth segmentation solutions were collected from [24] and [25] respectively. The image dimension of 256 by 256 pixels was utilized for all test images. In addition, the test images had varying intensities to ensure that the proposed model met its objective in segmenting images with intensity inhomogeneity.

3.2 Local Image Fitting (LIF)

The LIF, which is important to handle images with intensity inhomogeneity, was computed using the LIF model [13]. Assuming that for an image $I = I(x, y)$ in a domain Ω, the LIF energy function in the level set formulation, $E_{\varepsilon}^{LIF}(\phi)$ is defined as follows:

$$E_{\varepsilon}^{LIF}(\phi) = \frac{1}{2}\int_{\Omega} \left| I - I^{LIF} \right|^2 dxdy \tag{1}$$

Here, the function $\phi(x, y)$ is a level set function that represents the segmentation contour. The fitted image $I^{LIF} = I^{LIF}(x, y)$ in equation (1) can be written as $I^{LIF} = n_1 H(\phi) + n_2(1 - H(\phi))$ where $H(\phi)$ is a heaviside function or also known as the characteristics function. The value $H(\phi)$ is 1 inside the contour and 0 outside the contour. Next, $n_1 = \text{mean}\left(I \in \left(\left\{(x, y) \in \Omega \middle| \phi < 0\right\} \cap W_k\right)\right)$ and $n_2 = \text{mean}\left(I \in \left(\left\{(x, y) \in \Omega \middle| \phi < 0\right\} \cap W_k\right)\right)$ are the intensity averages of interior and exterior in a local region respectively.

3.3 Distance Function (DF)

In the GRSS model [23], the marker set was introduced, and it was defined as $A = \left\{w_i = (x_i^*, y_i^*) \in \Omega, 1 \le i \le n_1\right\}$ with n_1(≥3) marker points that were placed near the targeted object. Then, the DF which is the Euclidean distance of each point $(x, y) \in \Omega$ from its nearest point in the polygon, P made up of $(x_p, y_p) \in P$, constructed from the user input set, A was defined as follows:

$$P_d(x, y) = \sqrt{\left(x - x_p\right)^2 + \left(y - y_p\right)^2} \tag{2}$$

Here, the DF was introduced as a penalty term so that the evolving segmentation contour remains close to the targeted object indicated by the marker set.

3.4 Total Variation (TV) Term

In modeling an ACM, the TV term is used to regularize the generated segmentation curve. One of the earliest ACM that utilized the TV term is the CV model [11]. The TV term was defined as follows:

$$TV = \int_{\Omega} \delta(\phi) \left|\nabla \phi\right| \, dxdy \tag{3}$$

Here, the function $\delta(\phi)$ is the Dirac delta functional which is equivalent to $H'(\phi)$ and the function $\left|\nabla \phi\right|$ is the magnitude of gradient ϕ. By minimizing the TV term, the length of the generated curve was optimized to ensure it is short and smooth. Although the CV model applies to the TV term, the generated segmentation curve by the model was over-segmented especially in segmenting one object among other objects. This was mainly because the model is a global type of segmentation model.

3.5 Total Energy Function

The proposed TVSS model was formulated by modeling a total energy minimization function that utilized the LIF energy, DF, and TV term. As a result, the proposed TVSS model was defined as follows:

$$\min_{\phi}\left\{ \; TVSS(\phi)=\nu\int_{\Omega}\delta(\phi)|\nabla\phi| \; dxdy+\frac{1}{2}\int_{\Omega}\Big(I-\big(n_1H(\phi)+n_2\left(1-H(\phi)\right)\big)\Big)^2 \; dxdy \right. \\ \left. +\theta\int_{\Omega}P_dH(\phi)\,dxdy \; \right\} \tag{4}$$

with $n_1(x,y)=k_\sigma*\left[H(\phi)I\right]/k_\sigma*H(\phi)$ and $n_2(x,y)=k_\sigma*[1-H(\phi)]I/k_\sigma*[1-H(\phi)]$. The function k_σ is a Gaussian kernel with standard deviation σ such that $k_\sigma=e^{-(x^2+y^2)/2\sigma^2}$. The parameter θ restricts the contour from evolving too far from the targeted object. Normally, smaller θ is suitable if the targeted object can be clearly distinguished form the background and vice versa [26-27]. To obtain a smooth contour, the TV term which is the first integrand was used to regularize the generated segmentation curve. The term was weight by the parameter ν. For noisy images, a large ν can be imposed.

3.6 Derivation of Euler Lagrange Partial Differential Equation (EL-PDE)

The proposed TVSS model in equation (4) was minimized using calculus of variation by deriving its EL-PDE. Firstly, n_1 and n_2 was kept fixed and minimized the equation (4) with respect to ϕ using the Gateaux derivative. In calculus of variation, the Gateaux derivative is used to find the first variation of the model formulation function with respect to ϕ. The Gateaux derivative of $TVSS$ at a point ϕ and a test function ψ, denoted by $\frac{\partial}{\partial\phi}TVSS(\phi,\psi)$, is defined as the limit which is illustrated in the following equation (5).

$$\frac{\partial}{\partial\phi}TVSS(\phi,\psi)=\lim_{h\to 0}\frac{TVSS(\phi+h\psi)-TVSS(\phi)}{h}=\frac{d}{dh}TVSS(\phi+h\psi)\Big|_{h=0} \tag{5}$$

Thus, by applying the equation (5), we arrived at the following equation (6):

$$\frac{d}{dh}\int_{\Omega}\frac{1}{2}\Big[I-\big(n_1H(\phi+h\psi)+n_2\left(1-H(\phi+h\psi)\right)\big)\Big]^2\,dxdy\Big|_{h=0} \\ +\frac{d}{dh}\int_{\Omega}\theta P_dH(\phi+h\psi)\,dxdy\Big|_{h=0}+\frac{d}{dh}\nu\int_{\Omega}\delta(\phi+h\psi)\left|\nabla(\phi+h\psi)\right|dxdy\Big|_{h=0} \tag{6}$$

Differentiating all the integrands involved in equation (6) yielded:

$$\int_{\Omega}\Big[I-\big(n_1H(\phi+h\psi)\big)+n_2\left(1-H(\phi+h\psi)\right)\Big]\Big[-n_1H'(\phi+h\psi)\psi+n_2H'(\phi+h\psi)\psi\Big]d\Omega\Big|_{h=0} \\ +\int_{\Omega}\nu\delta(\phi+h\psi)\frac{d}{dh}\big(\left|\nabla(\phi+h\psi)\right|\big)d\Omega\Big|_{h=0}+\int_{\Omega}\left|\nabla(\phi+h\psi)\right|\nu\frac{d}{dh}\delta(\phi+h\psi)\,d\Omega\Big|_{h=0} \\ +\int_{\Omega}\theta P_dH'(\phi+h\psi)\psi d\Omega\Big|_{h=0}$$

After simplification, we obtained the following equation (7) as follows:

$$\int_{\Omega}\delta(\phi)\psi\Big[I-\big(n_1H(\phi)+n_2\left(1-H(\phi)\right)\big)\Big]\left[-n_1+n_2\right]dxdy+\int_{\Omega}\nu\delta(\phi)\frac{\nabla\phi\cdot\nabla\psi}{|\nabla\phi|}dxdy \\ +\int_{\Omega}\nu|\nabla\phi|\delta'(\phi)\psi dxdy+\int_{\Omega}\theta P_d\delta(\phi)\psi dxdy=0 \tag{7}$$

Green's theorem was applied to further simplify the equation (7) that yielded the following equation (8):

$$\int_{\Omega}\delta(\phi)\psi\Big[I-\big(n_1H(\phi)+n_2\left(1-H(\phi)\right)\big)\Big]\left[-n_1+n_2\right]dxdy- \\ \int_{\Omega}\nu\psi\delta(\phi)\nabla\cdot\frac{\nabla\phi}{|\nabla\phi|}dxdy+\int_{\partial\Omega}\nu\psi\frac{\delta(\phi)}{|\nabla\phi|}\cdot\frac{\partial\phi}{\partial n}dS+\int_{\Omega}\theta P_d\delta(\phi)\psi dxdy \tag{8}$$

Here, n is the unit normal vector and S is the arc length. Note that the EL-PDE is defined when $\frac{\partial}{\partial\phi}TVSS(\phi,\psi)=0$. Thus, for all test function ψ, the integrands in equation (8) will be zero if

$$\delta(\phi)\Big[I-\big(n_1H(\phi)+n_2(1-H(\phi))\big)\Big][-n_1+n_2]-\nu\delta(\phi)\nabla\cdot\frac{\nabla\phi}{|\nabla\phi|}+\theta P_d\delta(\phi) \tag{9}$$

with Neumann Boundary condition such that $\frac{\partial\phi}{\partial n}\left[\nu\frac{\delta(\phi)}{|\nabla\phi|}\right]=0\Rightarrow\frac{\partial\phi}{\partial n}=0$. Here, equation (9) is called the EL-PDE of the proposed TVSS model.

3.7 Solving the EL-PDE of the Proposed TVSS Model

To solve the EL-PDE in equation (9) iteratively, the gradient descent method is applied where an artificial time step t is introduced such that

$$\begin{aligned}\frac{\partial\phi}{\partial t}&=-\frac{\partial}{\partial\varphi}TVSS\\ &=\delta(\phi)\Big[I-\big(n_1H(\phi)+n_2(1-H(\phi))\big)(n_1-n_2)\Big]+\nu\delta(\phi)\nabla\cdot\frac{\nabla\phi}{|\nabla\phi|}-\theta\delta(\phi)P_d\end{aligned} \tag{10}$$

Equation (10) was discretized and solved using the explicit finite difference scheme using the following equation (11).

$$\begin{aligned}\phi_{i,j}^{n+1}=\phi_{i,j}^{n}+\Delta t\{\ &\delta\left(\phi_{i,j}^{n}\right)\Big[I-\Big(n_1H\left(\phi_{i,j}^{n}\right)+n_2\Big(1-H\left(\phi_{i,j}^{n}\right)\Big)\Big)(n_1-n_2)\Big]\\ &+\nu\delta\left(\phi_{i,j}^{n}\right)\nabla\cdot\frac{\nabla\phi_{i,j}^{n}}{\left|\nabla\phi_{i,j}^{n}\right|}-\delta\left(\phi_{i,j}^{n}\right)[\theta P_d]\ \}\end{aligned} \tag{11}$$

3.8 Performance Comparison

The segmentation performance was judged based on the quantitative accuracy measures using the Dice Similarity Coefficient (DSC) and Jaccard Similarity Coefficient (JSC) metrics. The metrics were computed based on the following formulae:

$$\text{JSC}=\frac{|S_n\cap S_*|}{|S_n\cup S_*|},\ \text{DSC}=\frac{|S_n\cap S_*|}{|S_n|+|S_*|} \tag{12}$$

where S_n is the set of segmentation domain generated by GRSS or TVSS model and S_* is the ground truth solution domain. The return value of DSC and JSC that approaches 1 indicates good quality segmentation. The value that approaches 0 indicates poor segmentation quality. The processing time was also recorded to determine the efficiency of the GRSS model and the TVSS model.

3.9 TVSS Model's Algorithm

To compute the solution of equation (11), the MATLAB R2017b software was used in a laptop with the specification of Processor: Intel(R) Core(TM) i7- 6500 CPU @ 2.50GHz 2.60 GHz installed memory (RAM): 8 GB, System type: 64 - boy operating system, 64-based processor. The following Figure present the algorithm to implement the TVSS model.

1. Input the test image.
   >> *Img = imread('image.png');*
2. Set values of *tol*, *maxit*, σ and θ.
   >> *maxit = 100; tol=1e-6; theta=20; sigma =90;*
3. Marker set is defined around the targeted object.
   >> *mx = [125;62;97;158;214;174]; my = [56;120;147;161;150;62];*
4. For iteration=1 to *maxit* or $\|\phi^{n+1} - \phi^n\|/\|\phi^n\| \leq tol$ do
   Generate the function ϕ which is the zero-level set function based on Equation (11).
   >> *for iteration = 1: maxit*
   >> *[phi]= TVSS(Img,mx,my,theta,sigma,maxit,tol);*
   >> *R=Residual(phi,oldphi)/norm(oldphi);*
   >> *if R<tol, break, end*
   >> *end*
5. The final segmentation curve will be the output ϕ.
   >> *figure, imagesc(phi);colormap gray;*

Figure 1. Steps to implement the TVSS model

4. Results and Discussion

Figure 2 shows all 12 sets of test images with the initial contour in yellow and marker set in green used in this experiment.

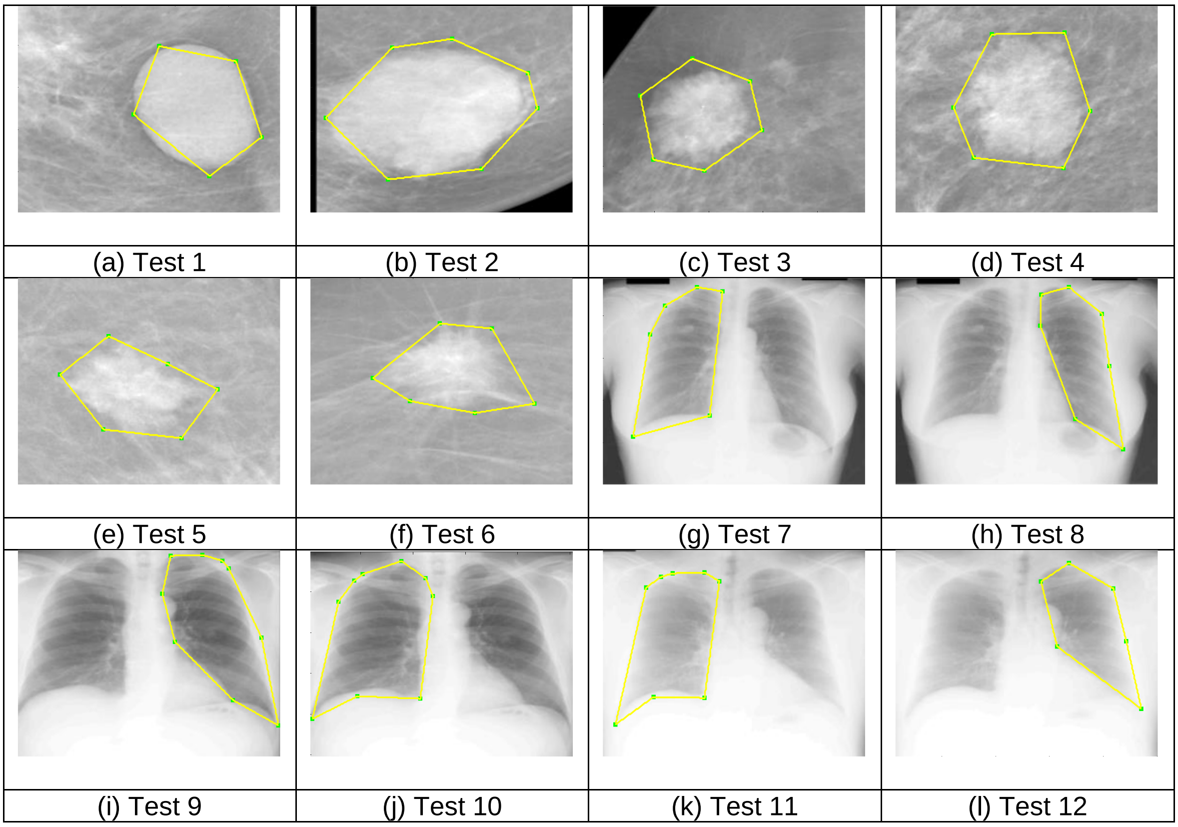

Figure 2. Test images with initial contours and marker set

From Figure 2, Test 1 until Test 6 were mammography images, while Test 7 until Test 12 were chest x-ray images. These types of images were chosen because all the test images were challenging to be segmented due to low contrast appearance. Additionally, the images had inhomogeneous intensity. Hence, all the images chosen were significant in testing the performance of the proposed model. The segmentation process was run using the MATLAB software, and the segmentation results of all test images were compared between the proposed TVSS model and the GRSS model [24].

4.1 Segmentation of Mammography Images

The visual illustration of the segmentation result for the mammography images are demonstrated in the following Figure 3.

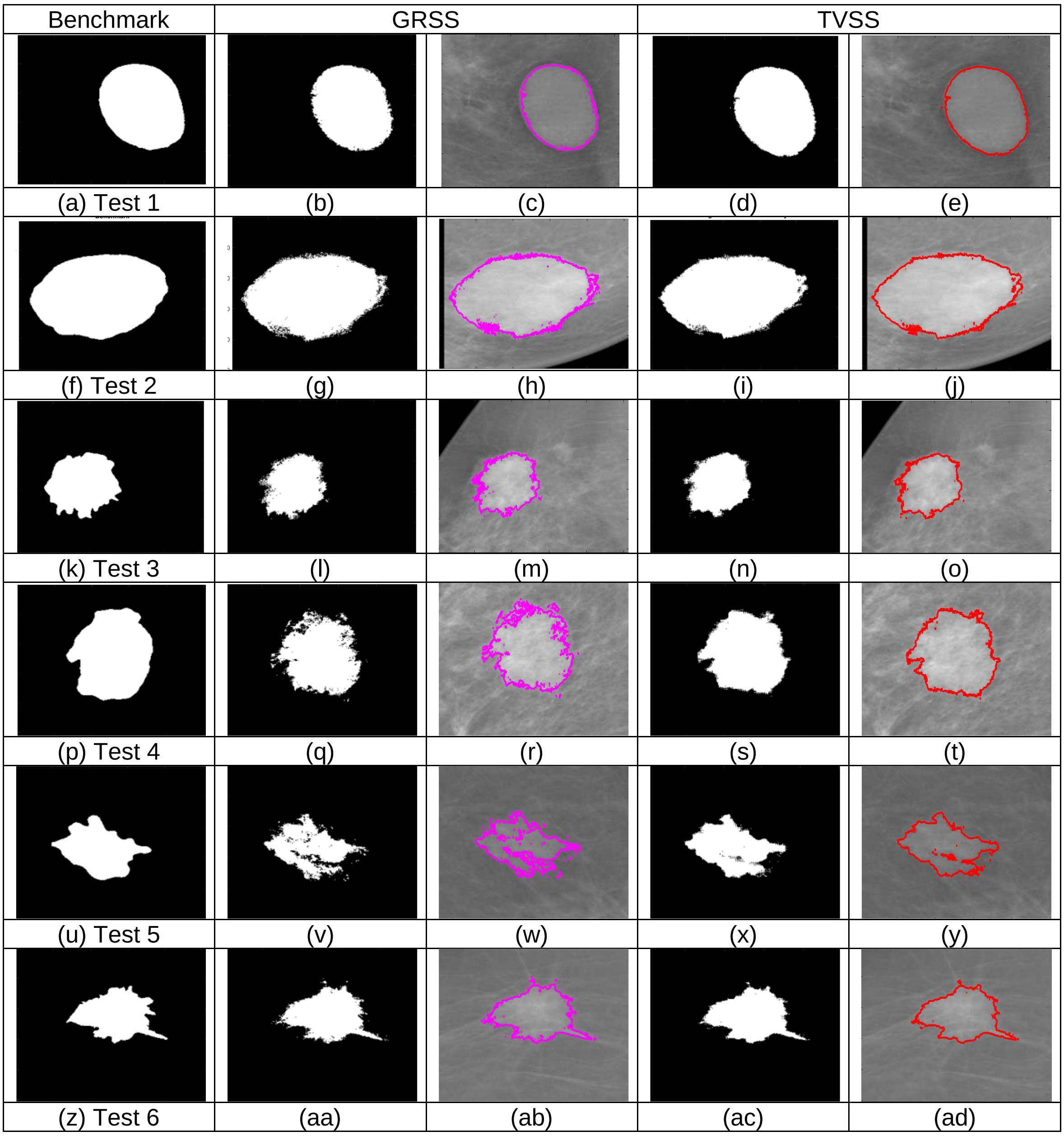

Figure 3. Segmentation results from GRSS model and TVSS model in segmenting mammography images

As shown in Figure 3, the benchmarks (ground truth solutions) of the test mammography images are shown in the first column. There are two types of results generated from each model. The first type is the binary form as shown in the second and fourth columns which represent the results by the GRSS model and TVSS model respectively. The second type is the contour or curve representation as demonstrated in the third and last columns which demonstrate the results generated by GRSS model and TVSS model respectively.

By visual observation, both models were able to segment the targeted region (breast abnormalities) of all the test images. However, both produced different segmentation results. For instance, it is clear that the segmentation results for the GRSS model in Figure 3 (m, r and w) produced large amounts of unnecessary artifacts, which made the final contour more scattered. On the other hand, the result produced by the proposed TVSS was smoother as indicated in Figure 3 (o, t and y). These results demonstrate the advantage of using the TV term in the proposed TVSS model compared to the Gaussian regularization term utilized in the GRSS model. By incorporating the TV term in the TVSS model, the length of the segmentation curve was minimized that gave a smoothing effect to the final segmentation curve.

Besides the qualitative visual observation, this experiment was also judged based on the quantitative accuracy measures using the Dice Similarity Coefficient (DSC) and Jaccard Similarity Coefficient (JSC) metrics. Additionally, the processing time was also recorded to determine the efficiency of the GRSS model and the TVSS model. Table 1 demonstrates the JSC, DSC and processing time of both models in segmenting all mammography test images.

Table 1. JSC, DSC and Processing Time for Segmenting Mammography Images

Image	**JSC**		**DSC**		**Processing Time**	
	GRSS	TVSS	GRSS	TVSS	GRSS	TVSS
Test 1	0.8944	0.9335	0.9443	0.9656	38.0244	9.4841
Test 2	0.8976	0.9032	0.9460	0.9491	71.8910	83.9554
Test 3	0.7779	0.7946	0.8751	0.8856	21.9318	22.3152
Test 4	0.7383	0.8144	0.8495	0.8977	137.3918	136.3861
Test 5	0.7811	0.8845	0.8771	0.9387	11.3808	11.6315
Test 6	0.9132	0.9242	0.9547	0.9606	126.2228	127.4576
Average	0.8338	**0.8757**	0.9078	**0.9329**	67.8071	**65.2050**

From Table 1, by taking the average of the JSC and DSC values for both models in segmenting the object's boundaries in all mammography test images, it was observed that the average JSC and DSC values for the proposed model were 0.8757 and 0.9329, respectively, which were 4.78% and 2.69% higher than the average JSC and DSC values recorded in the GRSS model. It was also observed that the processing time for both models to obtain the final segmentation result was comparable.

4.2 Segmentation of Chest X-ray Images

Next, the performance of GRSS and the proposed TVSS models in segmenting the chest x-ray images were compared. The results are illustrated in Figure 4. A similar observation as in the previous experiment in segmenting mammography images was observed where the segmentation curves generated by the proposed TVSS model were smoother compared to the GRSS model. This was mainly because the proposed model utilized the TV term which was capable of regularizing contours effectively compared to the Gaussian term applied in the GRSS model. The results were also compared quantitively by measuring their JSC, DSC and processing time as tabulated in Table 2.

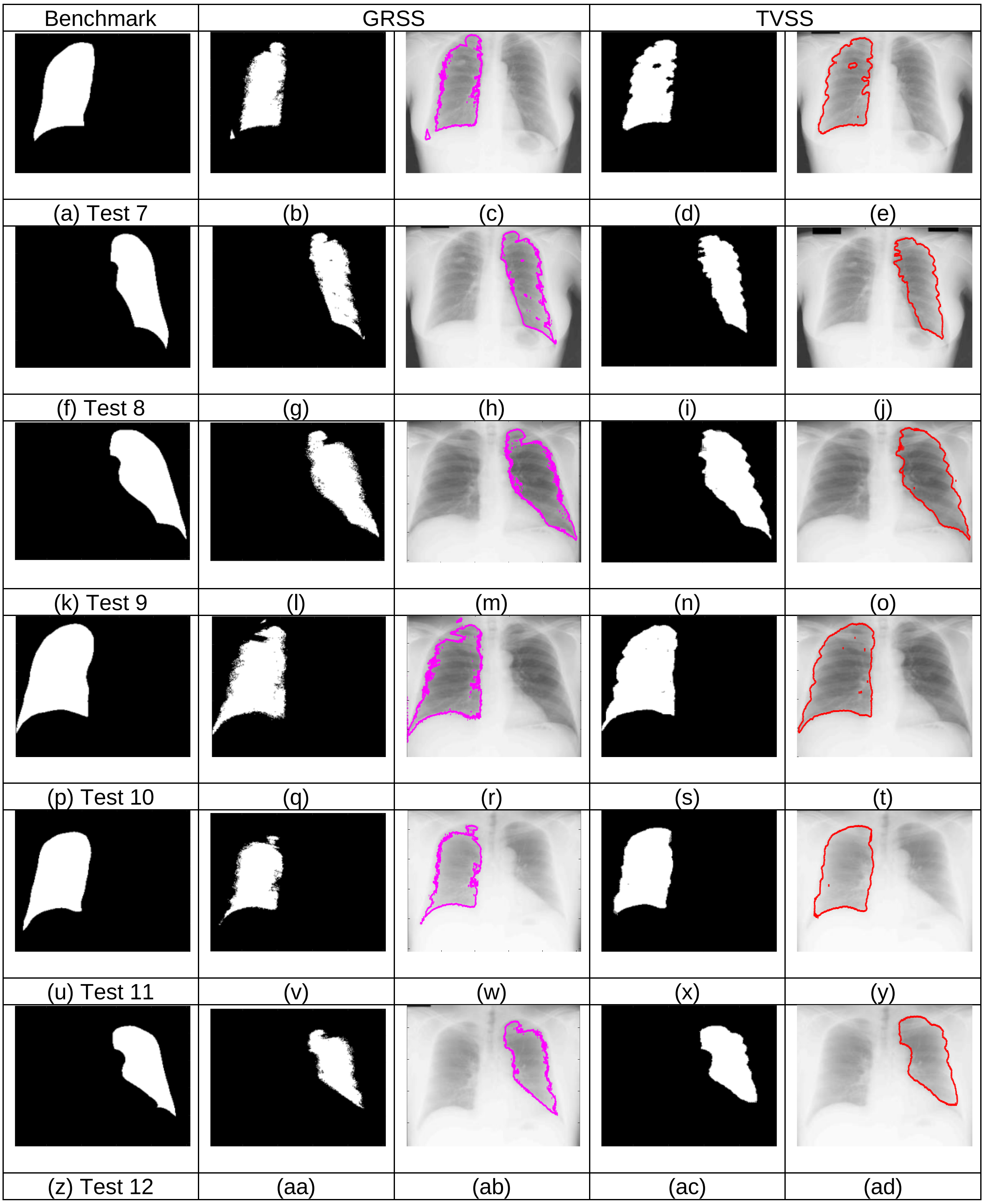

Figure 4. Segmentation results from GRSS model and TVSS model in segmenting chest X-ray images

Table 2. JSC, DSC and Processing Time for Segmenting Chest X-ray Images

Image	JSC		DSC		Processing Time	
	GRSS	TVSS	GRSS	TVSS	GRSS	TVSS
Test 7	0.7108	0.8355	0.8310	0.9104	16.5518	5.9613
Test 8	0.7507	0.7766	0.8576	0.8743	8.7095	6.0210
Test 9	0.7455	0.8650	0.8542	0.9276	16.6471	5.9322
Test 10	0.7958	0.9250	0.8863	0.9610	16.7538	5.8816
Test 11	0.7247	0.8751	0.8404	0.9334	16.7853	5.8733
Test 12	0.7013	0.8755	0.8244	0.9336	17.3944	5.8171
Average	0.7381	**0.8588**	0.8490	**0.9234**	15.4737	**5.9144**

As depicted in Table 2, By taking the average of the JSC and DSC values for both models in segmenting the object's boundaries in all chest X-ray test images, certain patterns were observed. The average JSC and DSC values for the proposed model were 0.8588 and 0.9234, respectively. These values were 14.05% and 8.06% higher than the average JSC and DSC values recorded in the GRSS model. It was also observed that the proposed model was more efficient than the GRSS model, as it took less time to obtain the final segmentation result as compared to the GRSS model.

5. Conclusion

A new variational selective region-based ACM called the TVSS model was developed in this study. It combined the TV term with local image intensities. The EL equation was derived to ensure optimality and was subsequently solved using MATLAB. The TVSS model was compared to the GRSS model in terms of segmentation accuracy and efficiency. Segmentation accuracy was assessed using the average JSC and DSC values, while processing time was recorded to evaluate segmentation efficiency. All models successfully segmented the specified items visually, as indicated by the findings. However, the TVSS model was able to generate a smoother segmentation curve compared to the GRSS model. Additionally, the proposed TVSS model had the highest accuracy with a comparable processing time. The proposed TVSS model can be potentially commercialized by developing a software for image analysis that serves as a second eye to physicians or radiologists in interpreting a medical image for further decision. To enhance accuracy, the concept of saliency from references [28-29] can be included in future work.

Acknowledgements

The authors gratefully acknowledge the Universiti Teknologi MARA (UiTM), Negeri Sembilan branch and UiTM Shah Alam for supporting this research.

Conflict of Interest

The authors declare no conflict of interest in the subject matter or materials discussed in this manuscript.

References

[1] S. N. Kumar, A. Lenin Fred, H. Ajay Kumar, and P. Sebastin Varghese, "Performance metric evaluation of segmentation algorithms for gold standard medical images," in *Adv. Intell. Syst. and Comput.*, vol. 709, 2018, pp. 457–469, doi: 10.1007/978-981-10-8633-5_45.

[2] N. Ismail, A. K. Jumaat, and N. F. A. Zulkarnain, "An Improved Variational-Based Model for Denoising and Segmentation of Vector-Valued Images," *J. Adv. Res. Appl. Sci. Eng. Tech.*, vol. 40, no. 1, pp. 189–203, 2024.

[3] M. S. Mazlin, A. K. Jumaat, and R. Embong, "Partitioning intensity inhomogeneity colour images via Saliency-based active contour," *International Journal of Electrical and Computer Engineering (IJECE)*, vol. 14, no. 1, pp.337–346, 2024.

[4] N. A. Kon, A. K. Jumaat, and M. D. A. Suhaizi, "Active Contour Models for Boundary Extraction with Application to Medical Images with Noise," *J. Adv. Res. Appl. Sci. Eng. Tech.*, vol. 33, no. 2, pp. 300–312, 2024.

[5] M. S. Mazlin, A. K. Jumaat, and R. Embong, "Saliency-based variational active contour model

for image with intensity inhomogeneity," *Indonesian Journal of Electrical Engineering and Computer Science*, vol. 32, no. 1, pp.206–215, 2023.

[6] M. Kass, A. Witkin, and D. Terzopoulos, "Snakes: Active contour models," *Int. J. comput. vision*, vol. 1, pp. 321-331, 1988, doi:10.1007/BF00133570.

[7] S. Osher and J. A. Sethian, "Fronts propagating with curvature-dependent speed: Algorithms based on Hamilton-Jacobi formulations," *J. comput. phys.*, vol. 79, pp. 12-49, 1988, doi:10.1016/0021-9991(88)90002-2.

[8] H. Ali, L. Rada and N. Badshah, "Image Segmentation for Intensity Inhomogeneity in Presence of High Noise," *IEEE Transactions on Image Processing*, vol. 27, pp. 3729-3738, 2018, doi:10.1109/TIP.2018.2825101.

[9] S. Soomro, A. Munir and K. N. Choi, "Fuzzy c-means clustering based active contour model driven by edge scaled region information," *Expert Syst. with Appl.*, vol. 120, pp. 387-396, 2019, doi:10.1016/j.eswa.2018.10.052.

[10] D. B. Mumford and J. Shah, "Optimal approximations by piecewise smooth functions and associated variational problems," *Commun. Pure and Appl. Math.*, vol. 42, pp. 577-685, 1989, doi:10.1002/cpa.3160420503.

[11] T. F. Chan and L. A. Vese, "Active contours without edges," *IEEE Transactions on Image Processing*, vol. 10, pp. 266-277, 2001, doi:10.1109/83.902291.

[12] C. Li, C. Y. Kao, J. C. Gore and Z. Ding, "Implicit Active Contours Driven by Local Binary Fitting Energy," In *Proc. IEEE Conf. Comput. Vision and Pattern Recognit.*, 2007, pp. 1-7, doi: 10.1109/CVPR.2007.383014.

[13] K. Zhang, H. Song and L. Zhang, "Active contours driven by local image fitting energy," *Pattern Recognit.*, vol. 43, pp. 1199-1206, 2010, doi:10.1016/j.patcog.2009.10.010.

[14] H. Wang, and T. Z. Huang, "An adaptive weighting parameter estimation between local and global intensity fitting energy for image segmentation," *Commun in Nonlinear Sci. and Numer. Simul.*, vol. 19, pp. 3098-3105, 2014, doi:10.1016/j.cnsns.2014.02.015.

[15] Y. Yang, W. Jia and B. Wu, "Simultaneous segmentation and correction model for color medical and natural images with intensity inhomogeneity," *The Visual Comput.*, vol. 36, pp. 717-731, 2020, doi:10.1007/s00371-019-01651-4.

[16] E. Iqbal *et. al.,* "Saliency-driven active contour model for image segmentation," *IEEE Access*, vol. 8, pp. 208978-208991, 2020, doi: 10.1109/ACCESS.2020.3038945.

[17] N. F. Idris, M. A. Ismail, M. S. Mohamad, S. Kasim, Z. Zakaria, and T. Sutikno, "Breast cancer disease classification using fuzzy ID3 algorithm based on association function," *IAES Int. J. Artif. Intell. (IJ-AI)*, vol. 11, no. 2, pp. 448, Jun. 2022, doi: 10.11591/ijai.v11.i2.pp448-461.

[18] H. M. Ahmed and M. Y. Kashmola, "A proposed architecture for convolutional neural networks to detect skin cancers," *IAES Int. J. Artif. Intell. (IJ-AI)*, vol. 11, no. 2, pp. 485, Jun. 2022, doi: 10.11591/ijai. v11.i2.

[19] A. H. T. Al-Ghrairi, A. A. Mohammed, and E. Z. Sameen, "Face detection and recognition with 180 degree rotation based on principal component analysis algorithm," *IAES Int. J. Artif. Intell.*, vol. 11, no. 2, pp. 593–602, 2022, doi: 10.11591/ijai.v11.i2.pp593-602.

[20] M. Z. Ansari, T. Ahmad, M. M. S. Beg, and N. Bari, "Language lexicons for Hindi-English multilingual text processing," *IAES Int. J. Artif. Intell. (IJ-AI)*, vol. 11, no. 2, pp. 641, 2022, doi: 10.11591/ijai. v11.i2. pp641-648.

[21] A. K. Jumaat and K. Chen, K, "A reformulated convex and selective variational image segmentation model and its fast multilevel algorithm," *Numerical Mathematics Theory Methods and Applications*, vol. 12, no. 2,pp. 403–437, 2019, doi: 0.4208/nmtma.OA-2017-0143.

[22] N. A. S. Mohd Ghani, A. K. Jumaat and R. Mahmud, "Boundary extraction of abnormality region in breast mammography image using active contours," *ESTEEM Academic J.*, vol. 18, pp.115-127, 2022.

[23] T. C. Saibin and A. K. Jumaat, "Variational selective segmentation model for intensity inhomogeneous image," *Indonesian J. Elect. Eng. and Comput. Sci.*, vol. 29, pp. 277-285, 2023, doi:1 10.11591/ijeecs.v29.i1.

[24] I. C. Moreira, I. Amaral, I. Domingues, A. Cardoso, M. J. Cardoso and J. S. Cardoso, "Toward a Full-field Digital Mammographic Database. Academic Radiology," Sep 2011, Distributed by INbreast. vol 19, no. 2, pp. 236–248. https://doi.org/10.1016/j.acra.2011.09.014.

[25] S. Candemir, S. Jaeger, K. Palaniappan, J.P. Musco, R. K. Singh, Z. Xue, A. Karargyris, S. Antani, G. Thoma and C. J. McDonald, "Lung segmentation in chest radiographs using anatomical atlases with nonrigid registration," *IEEE Trans Med Imaging*, vol. 33, no. 2, pp.

577-90, 2014, doi: 10.1109/TMI.2013.2290491. PMID: 24239990.
[26] A. K. Jumaat and K. Chen, "Three-dimensional convex and selective variational image segmentation model," *Malaysian Journal of Mathematical Sciences*, vol. 14, no. 3, pp. 437–450, 2020, https://einspem.upm.edu.my/journal/fullpaper/vol14no3/7.%20Abdul%20Kadir%20Jumaat.pdf.
[27] A. K. Jumaat and K. Chen, "An optimization-based multilevel algorithm for variational image segmentation models," *Electronic Transactions on Numerical Analysis*, vol. 46, pp. 474–504, 2017, https://etna.ricam.oeaw.ac.at/vol.46.2017/pp474-504.dir/pp474-504.pdf.
[28] P. T. Krishnan, P. Balasubramanian, V. Jeyakumar, S. Mahadevan and A. Noel Joseph Raj, "Intensity matching through saliency maps for thermal and visible image registration for face detection applications," *Vis Comput.,* pp. 1–14, 2022, doi: 10.1007/s00371-022-02605-z.
[29] V. Lukin, E. Bataeva and S. Abramov, "Saliency map in image visual quality assessment and processing," *Radioelectronic and Computer Systems*, vol. 1, pp. 112–121, 2023, doi: 10.32620/reks.2023.1.09.

Biography of all authors

Picture	Biography	Authorship contribution
	**Nadiah Mohamed** obtained the B.Sc. degrees in Mathematics from the Universiti Teknologi MARA, (UiTM) Shah Alam, Malaysia and M.Sc. in Mathematics from Universiti Kebangsaan Malaysia. Presently, she holds the position of senior lecturer at the School of Mathematical Sciences in UiTM Negeri Sembilan Kampus Kuala Pilah, Malaysia. Her research interests include operational research, image/signal processing, and medical image analysis. Her email address is nadiah@uitm.edu.my.	Design the research work, data collection, data analysis and interpretation, drafting article.
	**Abdul Kadir Jumaat** obtained the B.Sc. and M.Sc. degrees in Mathematics from the UiTM Shah Alam, Malaysia and the University of Liverpool, in United Kingdom, awarded him a Ph.D. degree particularly in Applied Mathematics. Presently, he holds the position of senior lecturer at the School of Mathematical Sciences and a research fellow at the Institute for Big Data Analytics and Artificial Intelligence (IBDAAI) in UiTM Shah Alam, Malaysia. His research interests include image/signal processing, artificial intelligence and computer vision. His email address is abdulkadir@tmsk.uitm.edu.my	Design and supervising the research work and camera ready.
	**Rozi Mahmud** obtained the medical degree in University of Malaya. She subsequently went on to pursue her Masters in Radiology and obtained her MMed Rad from Universiti Kebangsaan Malaysia. She received a formal training at the Division of Neuroradiology and MRI at the Children's Hospital of Philadelphia and a formal training for mammogram and breast biopsy from L'Istituto Nazionale di Fisica Nucleare INFN, Sezione in Torino Italy. Presently, she holds the position of Professor and Director, Centre for Diagnostic Nuclear Imaging, Universiti Putra Malaysia. Her research interests include Radiology / Neuroradiology/Breast Disease/AI in medical Imaging. Her email address is rozi@upm.edu.my	Supervising the research work